THE JOURNAL OF PHYSICAL CHEMISTRY B

Article

pubs.acs.org/JPCB

Role of Tunneling in the Enzyme Glutamate Mutase

Judith B. Rommel, Yu Liu, Hans-Joachim Werner, and Johannes Kästner*

Institute of Theoretical Chemistry, University of Stuttgart, Pfaffenwaldring 55, D-70569 Stuttgart, Germany

Supporting Information

ABSTRACT: The role of quantum mechanical atom tunneling during the conversion of glutamate to methylaspartate catalyzed by glutamate mutase is investigated by quantum mechanical/molecular mechanical (QM/MM) simulations based on coupled cluster and density functional calculations. The use of instanton theory allows us to calculate the tunneling contributions of up to 78 atoms in the active site. We calculate kinetic isotope effects (KIEs) and compare them to experimental data. The simulations lead to deuterium KIEs of 10 for the hydrogen abstraction from glutamate substrate and 16 for the hydrogen abstraction from methylaspartate substrate, which are consistent with the experimental results. The hydrogen abstraction from methylaspartate has higher primary deuterium and tritium (46.1) KIEs than the abstraction from glutamate. The tunneling effect increases the reaction rate by a factor of 12.3 for the hydrogen abstraction from methylaspartate at 0. Tunneling is supported by the environment by preparing the enzyme through classical motions. Consideraton of the tunneling contributions of more and more atoms around the active center shows that the motions at the ribose ring play a central role during the tunneling enhancement of the hydrogen transfers. Our simulations give new insight into the catalytic process in glutamate mutase and the way enzymes use tunneling effects for a successful catalysis.

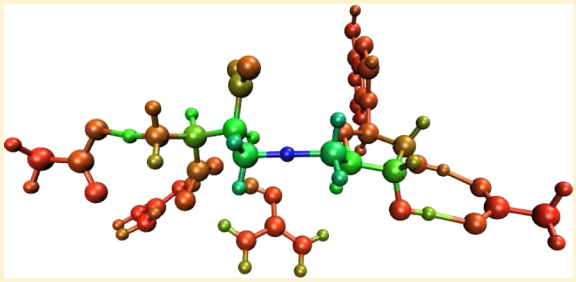

1. INTRODUCTION: TUNNELING IN GLUTAMATE MUTASE?

Atom tunneling is involved in many chemical reactions that include hydrogen transfers. It is a quantum mechanical effect by which particles penetrate classically forbidden regions of coordinate space and can cross energetic barriers that would be too high for nonquantum transitions. The smaller the mass and the lower and narrower the barrier, the larger is the tunneling probability.[1,2] Tunneling facilitates reactions compared to the classical over-the-barrier mechanism, especially at low temperature. However, in many enzymes tunneling of hydrogen atoms (H^+, H^-, or $H^\bullet$) can contribute to the reaction rate even at room temperature.[3−11] Kinetic isotope effects (KIEs) are used as experimental indicators to determine the contribution of tunneling.[12] The KIE is the ratio of the reaction rates with protium (H = ^{1}H) and a heavier isotopologue (containing deuterium, ^{2}H, or tritium, ^{3}H). Measurements of KIEs are powerful tools to study enzymatic reactions, because they demonstrate the contribution of specific atoms to the transition.[13−18] While a high KIE hints that tunneling enhances the rate-limiting step of the reaction, direct observation of atom tunneling is impossible by experiment alone. Computer simulations allow to switch the tunneling effect on and off and, thus, directly provide evidence of its contribution. Therefore, we use a simulation in this study to elucidate the tunneling behavior of an enzymatic system.

1.1. Reaction Catalyzed by Glutamate Mutase.

The enzyme glutamate mutase (GM) catalyzes the reversible interconversion of (*S*)-glutamate (Glu) to (2*S*,3*S*)-3-methylaspartate (MA).[19,20] GM uses 5′-deoxyadenosylcobalamin (AdoCbl), that is, coenzyme B_{12}, as cofactor.[21,22] The following intermediates of the fragmentation−recombination mechanism can be distinguished:[23−25] The resting state, denoted as A_0, is the inactive holoenzyme GM with AdoCbl as cofactor. Binding of the Glu substrate induces a homolytic cleavage of the cobalt−carbon bond of the cofactor, which yields a 5′-deoxyadenosyl radical (Ado) and cob(II)alamin,[26,27] state ***A*** (see Figure 1). Hydrogen atom transfer to Ado generates the glutamyl radical and Ado-H (5′-deoxyadenosine), state ***B***. Then follows the fragmentation into acrylate and a glycyl radical, state

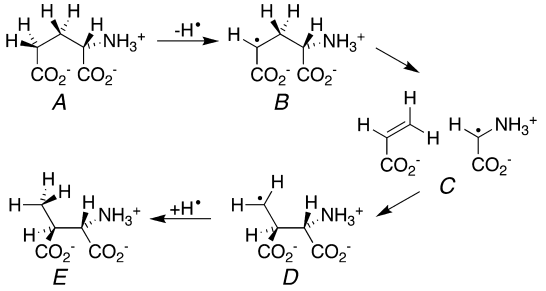

Figure 1. Rearrangement of glutamate to methylaspartate catalyzed by GM (A: 5′-deoxyadenosyl radical (Ado) and glutamate (Glu); B: Ado + H and glutamyl radical; C: Ado + H, acrylate, and glycyl radical; D: Ado + H and methylaspartyl radical; E: Ado and methylaspartate (MA)).

Received: August 28, 2012
Revised: November 5, 2012
Published: November 5, 2012

C. Binding glycyl to acrylate (recombination) results in the methylaspartyl radical, state *D*. The back-transfer of the hydrogen from Ado-H to the substrate yields MA, state *E*. The final part of the catalysis in GM is reforming the Co−C bond, resulting in E_0, and product release. The reaction is reversible; the forward and back reactions are studied here.

1.2. Experimental Reaction Rates and KIEs. Experimental measurements of rates and KIEs in GM were conducted with different techniques. All experimental data refer to a temperature of T = 283 K unless noted otherwise. The deuterium KIE for the complete interconversion from MA to Glu ($E_0 \rightarrow A_0$, MA triply deuterated at the active methyl group) was measured to be 6.3 ± 0.5.[28] Hydrogen abstraction from MA measured with an internal competition experiment resulted in a KIE of 4.1.[10,29] The KIE of the formation of Ado-H ($A_0 \rightarrow B$) measured directly by a competition experiment with trideuterated and unlabeled substrate in the same vessel was 10 ± 0.4.[30] However, the formation of cob(II)alamin ($E_0 \rightarrow E$) shows a KIE of 35.[31] As the deuterium KIEs measured in GM show a rather wide range from 4.1 to 35, it is unclear whether tunneling is involved in the mechanism of GM. Experiments investigating tritium isotope effects, based on rapid quench techniques,[30,32,33] resulted in KIEs of 21 and 19. A detailed overview on the results of different measurements in GM can be found in ref 34. We will in the following compare our computational results with these experiments.

The measurement of KIEs in biological systems remain a challenging issue. Experiments always result in apparent rates and KIEs that could be masked by experimental side effects like, for example, detection methods being insensitive to deuterium content below a certain threshold. Artifacts are also caused by multiple transfers of deuterium to the cofactor, which stays undetected when following the formation of cob(II)alamin. Above 283 K, the dideuteration of Ado-H increased rapidly to more than 2% of the yield, which rendered correct measurements of KIEs impossible.[30] The measurements are also limited to certain time frames as the threshold in concentration for detecting the substance of interest (e.g., the product) must be exceeded. In experimental investigations the back reaction affects the results, as GM catalyzes a reversible conversion. Thus, the measured rates are apparent ones leading to apparent KIEs. The intrinsic KIEs, real KIEs without masking side effects, can be obtained only indirectly by experiment. Computational approaches, however, allow to predict the intrinsic KIEs directly.

We used instanton theory[35−38] to investigate the role of tunneling during the reaction catalyzed by GM. To our knowledge this is the first study of tunneling in an enzyme with a fully optimized instanton approach.

The paper is organized as follows: In section II, methodological details, the level of theory, and the method employed to study tunneling in the enzyme based on rates and KIEs are given. In section III, we compare our density functional theory (DFT) and coupled cluster results concerning the energetics of the rearrangement reaction catalyzed by GM. Then the KIEs will be discussed and compared to experimental data. Then we discuss the influence and contributions of the neighboring atoms and amino acids to a productive catalysis. Finally, we speculate on a possible modulation of the rate determining step by isotopic replacement.

2. METHODS

2.1. Energies. In our previous study of the fragmentation−recombination mechanism of GM,[25] we used a combination of quantum chemical approaches and empiric force fields (QM/MM),[39,40] recently reviewed in refs 41−45. Here the same methods and the same system setup were used. The relative DFT energies were additionally validated against local coupled cluster reference calculations. All calculations here are based on a snapshot taken after 9 ns of classical molecular dynamics.[25] The QM/MM calculations were performed in ChemShell.[41] The CHARMM22 force field[46−49] in DL_POLY,[50] as included in ChemShell, was used for the MM part. The QM part comprised the Ado radical as part of the cofactor, the substrate, and part of the neighboring amino acid Glu 171 (*Clostridium cochlearium* notation), in total 54 atoms. Geometries were optimized using DFT[51,52] with the BP86[53−57] functional in TURBOMOLE version 6.0.2[58] in combination with density fitting (resolution of the identity)[59] and the cc-pVTZ[60] basis set. In our previous study[25] we showed that geometries obtained with BP86 hardly differ from those obtained by B3LYP. Relative QM/MM energies were then calculated on the BP86-geometry with the M06 functional[61] in NWChem version 5.1.1.[62,63] Now, we additionally calculate relative energies on the LUCCSD(T) (local unrestricted open-shell coupled cluster with single and double excitations and perturbative treatment of the triple excitations) level[64,65] with the aug-cc-pVTZ[60] basis set. A localization scheme, in which singly occupied and doubly occupied orbital space are treated separately, was used to avoid a mixing of the occupied RHF (restricted open-shell Hartree−Fock) orbital subspaces. The calculations were performed with Molpro version 2010.2.[66] The localization introduces a domain error, an error caused by restricting each pair of localized molecular orbitals to a subset (domain) of local virtual orbitals. The domain error was corrected for by the difference between the results for LRMP2 (local spin restricted open-shell second order Møller−Plesset perturbation theory)[64,65] and RMP2 (canonical spin restricted open-shell second order Møller−Plesset perturbation theory)[67] to the LUCCSD(T) results. Moreover, rates based on both M06 barriers and coupled cluster barriers are compared in the following. More details on the LUCCSD(T) results and the domain error correction are given in the Supporting Information.

2.2. Rates and KIEs. Instanton rate theory (also imaginary free energy method)[35−38] is a quantum rate theory based on statistical Feynman path integrals[68] to incorporate quantum tunneling effects. The instanton is the optimal tunneling path, the path with the highest statistical weight at a certain temperature. Fluctuations around this path are taken into account to second order. Due to its accuracy and applicability to large systems, the instanton method is increasingly used to calculate reaction rates in chemical systems.[69−87]

The instanton method is applicable only below the crossover temperature[88]

$$T_c = \frac{\hbar\omega_b}{2\pi k_B} \tag{1}$$

where $\hbar$ is Planck's constant, k_B is Boltzmann's constant, and ω_b is the magnitude of the imaginary frequency of the unstable mode at the saddle point. T_c can be interpreted as the temperature below which tunneling significantly contributes to the rate. In GM, T_c for the hydrogen-transfer reactions is above room temperature for the transfer of protium but below 273 K

for deuterium and tritium transfer. This makes instanton theory inapplicable in the latter cases. Thus, sixth-order Wigner corrections[89] were used in these cases. These show satisfactory agreement with instanton rates for protium transfer, see Figure 2, where the rates can directly be compared. Thus, we assume

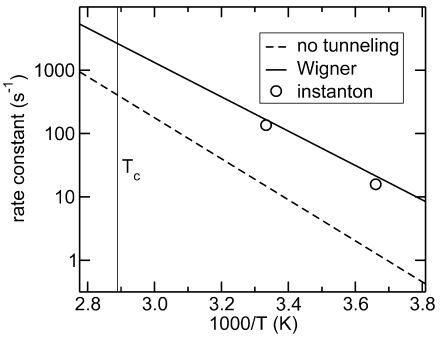

Figure 2. Rate constants (BP86/MM level) obtained from instanton theory compared to sixth-order Wigner correction for protium transfer in $E \rightarrow D$.

the Wigner correction to also reasonably describe deuterium and tritium transfer, for which instanton rates are not available. Sixth-order Wigner corrections are obtained by

$$\kappa(T) = 1 + \frac{1}{6}b^2 + \frac{7}{15}\frac{1}{4!}b^4 + \frac{31}{21}\frac{1}{6!}b^6 + O(\beta^8) \quad (2)$$

where $\beta = 1/(k_B T)$, $b = \beta\hbar\omega_b/2$, and $\kappa(T)$ is the tunneling correction factor. It is multiplied with the nontunneling rate to obtain an approximation for tunneling above T_c. Nontunneling rates denote rates by transition state theory with all vibrational modes of the QM/MM system treated as quantum mechanical harmonic oscillators, see eq 1 of the Supporting Information. These account for the zero-point energy, but not for tunneling. In the following, tunneling rates refer to instanton rates below T_c and rates obtained with sixth-order Wigner corrections above T_c. KIEs have to be calculated in several cases as ratios of rates obtained with these different theories.

The instanton path was optimized using a modified Newton−Raphson algorithm,[87] as implemented in DL-FIND.[90,91] The Feynman path was discretized into 5 distinct images that result in a closed path of 10 images (pairs of images are identical).[87] Hessians of the potential energy at each image were calculated from finite differences of gradients.

Instanton theory can be used with any kind of potential energy surface. Here, we use it with potential energies obtained on the fly from QM/MM calculations. It should be noted that the computational treatment of the electrons (atoms in the QM part vs the MM part) is independent of the computational treatment of the atomic movement (i.e., whether an atom is allowed to contribute to the tunneling). Throughout all the calculations, the QM part consisted of 54 atoms. However, to allow all atoms involved in the hydrogen transfer to tunnel, we varied the number of actively quantized atoms during the instanton optimizations and rate calculations. The number of tunneling atoms ranged from one, only the transferred hydrogen atom, to 78. The largest set is shown in Figure 3. All other atoms of the system were frozen at the TS geometry. The exact composition of the individual sets, rates, and KIEs are listed in the Supporting Information. In the following, results for rates and KIEs will refer to an active part consisting of 78 atoms unless stated otherwise.

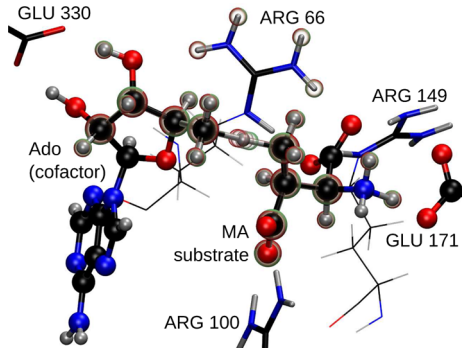

Figure 3. Large active region (78 atoms, $E \rightarrow D$) including the QM region (in ball and stick representation) consisting of Ado (left), MA substrate (middle), and the side chain of Glu 171 (right). Carbon is shown in gray, oxygen in red, nitrogen in blue, and hydrogen in white. Transparent spheres denote the movements of the most relevant tunneling atoms.

Rates were calculated at the BP86/MM level with corrections for the barrier height by M06 and coupled cluster throughout. That is, instanton optimizations, the calculations of Hessians along the instanton path as well as the harmonic frequencies at the minima and saddle points were calculated by QM/MM based on the BP86 functional. Barrier heights from M06/MM and coupled cluster/MM were used for the rates by correcting the instanton rates by a factor $\exp(-\beta\Delta E)$. KIEs are independent of these barrier-height corrections as they cancel out in the ratio. Thus, the KIEs are obtained on the pure BP86/MM level.

3. RESULTS AND DISCUSSION

Minima are labeled according to Figure 1, as described in the Introduction. All transition states between the intermediates are abbreviated by TS, for example, TS-*DE* denotes the transition state between *D* and *E*. Energetic data for the different elementary reactions are given in Figure 4. Relative energies were consistently calculated with respect to the energy of the state *A*.

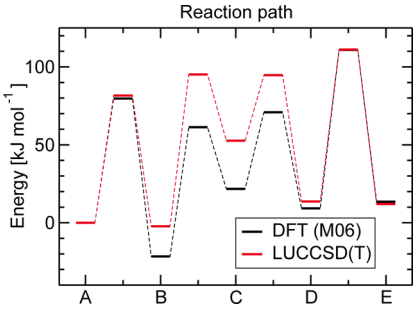

Figure 4. Comparison of the QM/MM potential energy profile with DFT (M06) and LUCCSD(T).

3.1. Energetics and Rates. The LUCCSD(T)/MM energies are compared to our previous DFT/MM results[25] in Figure 4 and Table 1. All energetic values refer to coupled cluster in the following unless noted otherwise. With coupled cluster as well as with DFT, *B* is the most stable intermediate. The barriers for the hydrogen-atom transfer reactions (transitions $A \rightarrow B$ and $E \rightarrow D$) remain almost unchanged by the change of the theoretical description. Tunneling can play

Table 1. Comparison of LUCCSD(T) with Domain Error Correction to DFT with the M06 Functional (QM/MM Energies in kJ mol^{-1} at BP86 Geometries)

structure	M06 cc-pVTZ	LUCCSD(T) aug-cc-pVTZ
A	0.0	0.0
TS-***AB***	79.7	81.6
B	−21.6	−2.3
TS-***BC***	61.3	95.1
C	21.7	52.6
TS-***CD***	70.9	94.6
D	9.2	13.6
TS-***DE***	110.9	111.0
E	13.5	12.0

a role during these two isotopically sensitive steps. The barriers for $A \rightarrow B$ and $D \rightarrow E$ differ by 29.4 kJ mol^{-1}, whereas the experimental investigations where tritium was transferred from Ado-H to form either Glu (substrate) or MA (product) resulted in a 1:1 distribution of tritium in the substrate and the product, which would mean that both barriers for transferring hydrogens are nearly equal.[92] This discrepancy may be caused by our MD simulations to prepare the QM/MM snapshots containing Glu in the binding pocket, that is, the QM/MM simulations started at ***A***. Our snapshots taken from MD simulations are frozen in the outer part of the enzyme, which might cause a bias increasing $D \rightarrow E$ relative to $A \rightarrow B$.

In the carbon skeleton rearrangement, the transition states for the fragmentation and recombination have about the same energy, 95.1 kJ mol^{-1} for $B \rightarrow C$ and 94.6 kJ mol^{-1} for $C \rightarrow D$. Apparently, in contrast to the experimental conclusion that "no single step was cleanly rate-limiting",[10,29] they differ significantly, by 15.9 and 16.4 kJ mol^{-1}, from the barriers of the hydrogen transfer $D \rightarrow E$. However, the direct reaction rate $E \rightarrow C$ (ignoring the barriers for the hydrogen transfer) is only 15.5 and 16.8 times higher (273.15 and 300 K, respectively) than $E \rightarrow D$. This translates to an energy difference of only 7 kJ mol^{-1} from the Arrhenius factor, possibly smaller than the accuracy of our QM/MM energies. How does the small difference in the rate come about with a rather large difference of 16.4 kJ mol^{-1} in the potential energies? The zero-point energy reduces the barrier for $E \rightarrow D$ by 12.3 kJ mol^{-1}, while it reduces the barrier $D \rightarrow C$ by only 3.8 kJ mol^{-1}.

The crossover temperatures T_c for the transitions from $A \rightarrow B$ are 307 K for protium, 232 K for deuterium, and 198 K for tritium transfers, consistent with the notion that tunneling is less important for the heavier isotopes. For the transitions form $E \rightarrow D$, the corresponding crossover temperatures are 346, 259, and 220 K, respectively. Atom tunneling increases the rate of the transition $E \rightarrow D$ by a factor of 12.3 for protium, 5.4 for deuterium, and 3.4 for tritium at 273.15 K. Notably, for the transition $A \rightarrow B$ tunneling speeds up the reaction only by a factor of 5.7 (protium). Thus, tunneling is less important for the hydrogen abstraction from Glu than from MA.

3.2. KIEs. Calculations and experimental measurements of KIEs are more accurate than rates. An isotopic substitution at an atom directly involved in establishing or breaking bonds during the reaction results in a primary KIE. In the following we will discuss our primary KIE results and compare to experiment. The results are summarized in Table 2.

With trideuterated Glu substrate the value of our primary deuterium KIE of 10.3 at 273.15 K for the transition $A \rightarrow B$ is in good agreement with the experimental result of 10 ± 0.4,[30] which was obtained by a competitive measurement (with both deuterated and unlabeled substrate in the same vessel) at 283 K, see Table 2. The higher KIE of 16.8 for $E \rightarrow D$ with trideuterated MA substrate supports the notion that tunneling is more important for the hydrogen abstraction from MA than from Glu.

Table 2. Primary Deuterium KIEs for the Hydrogen Transfers $A \rightarrow B$ and $E \rightarrow D$ on the Formation of Ado-H[10,29,30] or Cob(II)alamin[31]

	this work		experiment	
substrate	273.15 K	300 K	283 K	273 K
		Transition $A \rightarrow B$		
$^2H_3$-Glu	10.3	11.3	10 ± 0.4[30] 28[31]	
^{2}H-Glu	9.0	10.0		
		Transition $E \rightarrow D$		
$^2H_3$-MA	16.8	14.0	35[31]	
^{2}H-MA	13.5	11.5	4.1[29]	6[10]

Our deuterium KIEs for the transition $E \rightarrow D$ lie between the high and low measured KIEs given in Table 2, while some of the KIEs we obtain are higher than the experimental values. The large measured KIEs[31] seem to be sensitive to several side effects during the reaction and suffering from systematic error.[30] However, generally any masking of apparent KIEs in experiment leads to too low values of measured KIEs. Measuring thresholds, multiply deuterated substrates or the influence of the reverse reaction may mask KIEs. These effects are absent in our calculations.

Table 2 shows for the transition $A \rightarrow B$ an increase in the KIE with increasing temperature, which is in contrast to expectations. In this case, however, the instanton calculation for protium at 300 K, which enters both values for the KIE at 300 K, probably overestimates the reaction rate. The temperature of 300 K is very close to T_c = 307 K for that reaction. Instanton theory is known to overestimate rates close to T_c.[86] When all rates are calculated with sixth-order Wigner corrections the normal decreasing KIE with increasing temperature is found. This is not an issue for $E \rightarrow D$ because there T_c is 346 K significantly higher than 300 K.

Our primary tritium KIEs are compared to experiment in Table 3. Again, the calculated values are slightly higher than the measured ones, which may again be attributed to masking effects. The measurements of primary tritium KIEs used monotritiated AdoCbl and considered the transfer of tritium from Ado-H to Glu or MA substrate.

Table 3. Primary Tritium KIEs with Monotritiated Substrate

	this work		experiment
	273.15 K	300 K	283 K
$A \rightarrow B$	28.4	27.8	21[92]
$E \rightarrow D$	46.1	34.7	19[92]

The results for primary deuterium as well as for tritium KIEs confirm the conclusion drawn from the rates that tunneling is more important for the transition from $E \rightarrow D$ than for $A \rightarrow B$.

3.3. Participation of the Environment in the Tunneling Process. Our calculations provide the most likely tunneling path. The most likely reaction path from an energy minimum to the start of the tunneling path is provided by the intrinsic reaction coordinate (minimum energy path) between

dx.doi.org/10.1021/jp308526t | J. Phys. Chem. B 2012, 116, 13682−13689

these points. On average, the progress of the reaction is best described by the intrinsic reaction coordinate until the first caustic point, the start of the instanton path. Then the system tunnels to the second caustic point, the end of the instanton path and proceeds along the intrinsic reaction coordinate to the product minimum. This combined path is visualized in Figure 5

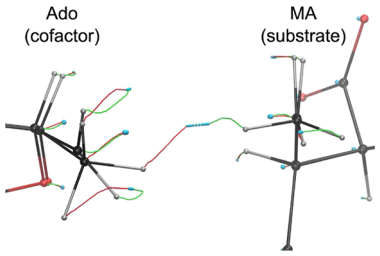

Figure 5. Most likely reaction path (intrinsic reaction coordinate and instanton path) of the transition ***D*** → ***E***. The nontunneling paths are denoted in red (start at ***D***) and green (end at ***E***). The blue balls between the red and green paths denote the instanton tunneling path.

for ***D*** → ***E*** at 273.15 K. The energy profile along that path (BP86/MM level) is illustrated in Figure 6. The heavy atoms

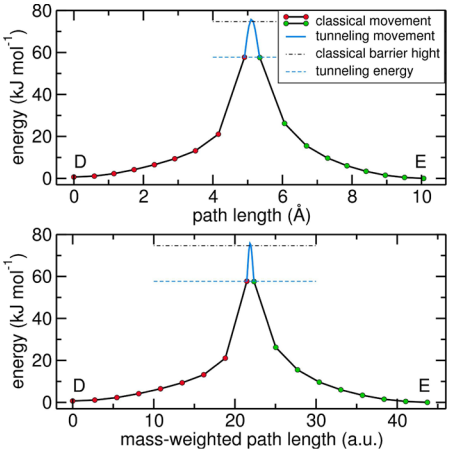

Figure 6. Energy profile (BP86/MM) along the most likely reaction path (intrinsic reaction coordinate, red and green dots, and instanton path, blue) of the transition ***D*** → ***E***. The path length covers all atoms.

dominate the classical movement. The system optimizes the tunneling path to mainly consist of hydrogen-atom movement. In Figure 5, this becomes apparent by the tunneling paths (blue dots) being of significant length only for the transferred hydrogen atom, while the red and green curves (classical paths) are long also for carbon atoms. The concentration of movement to the hydrogen atom is probably the reason why the simple Wigner approximation provides useful rates above T_c. Figure 6 compares the reaction path for all atoms in Cartesian coordinates to the path in mass-weighted Cartesian coordinates. The fact that the tunnel motion is dominated by hydrogen shortens the section of tunneling motion in the mass-weighted path compared to the Cartesian path length. The mass-weighted path length is the relevant quantity for the reaction rate.

Tunneling is rather weak, only a rather short portion of the reaction path is covered by tunneling motion. Also, energetically, the system moves up most of the barrier classically, while it tunnels only through the top. At much lower temperature (not accessible for enzymatic reactions) a larger fraction of the path would be covered by tunneling. The instanton path proceeds through a point slightly (1 kJ mol^{-1}) higher than the classical transition state, see Figure 6. This expense comes at the benefit of a shorter tunneling path, an effect known as corner cutting.[93]

It should be noted, of course, that what is shown here is only the most likely reaction path, which includes protium tunneling. In reality, the path as well as the tunneling energy will fluctuate. When our methods are used, such graphs can only be drawn for protium; instanton theory is applicable there. For deuterium and tritium in the primary position, the most likely tunneling energies lie above the classical barrier height, which makes instanton theory inapplicable in these cases, see section 2.

The atoms in the direct neighborhood of the transferred hydrogen at the Glu substrate and at the ribose ring of the adenosyl radical, and also, several hydrogen atoms on Arg 66 are involved in the most likely tunneling process ***D*** → ***E***, as illustrated in Figure 3 .

The secondary hydrogen atoms at the 5′-carbon atom of ribose influence the motions of the transferred primary hydrogen atom H_a. These atoms move from planar sp^2 to tetrahedral sp^3 geometry around the 5′-carbon. Their motions are coupled to the transition, see Figure 3, but only weakly, as can be seen by the short tunneling parts of these atoms in Figure 5. Such movements increase the effective mass (defined analogously to the effective mass in molecular vibrations) and reduce the tunneling efficiency. For the transition ***A*** → ***B***, the effective tunneling mass is μ_{eff} = 1.139 amu (atomic mass units, compared to 1.008 amu for a ^{1}H atom). In ***E*** → ***D***, it is slightly higher μ_{eff} = 1.163 amu. The motions are coupled to all transferred nuclides (protium, deuterium, and tritium) but have the highest effect on protium. Overall, our calculations hint that coupled motions are less important than previously thought.

To explore the influence of motions in the direct neighborhood of the active center on tunneling we restricted the tunneling to smaller sets of atoms, see description in section 2 and Supporting Information for more details. The larger the active subspace, the higher the effective mass during the transitions. The primary tritium KIE for ***E*** → ***D*** with only H_a allowed to tunnel is 39.9 at 273.15 K. This KIE is slightly smaller than the KIE of 46.1, see Table 3, for 78 tunneling atoms. The multiplicative factors between tunneling and nontunneling rates with only H_a allowed to tunnel are 3.36 for deuterium and 2.21 for tritium, much smaller than for the 78-atom set (with factors of 5.45 for ^{2}H and 3.40 for ^{3}H). Thus, for a successful tunneling contribution, the motions of the neighboring atoms are crucial to enhance the deuterium and tritium rates. For these two heavier isotopes the factors between tunneling and nontunneling rates are the same for all sets of tunneling atoms except for the set with only H_a included. The motions of the neighboring atoms are much more important for protium transfers than for its heavier isotopes. For ^{1}H the tunneling rate for one active atom is 4.58 times faster than the nontunneling rate. For the large active space with 78 atoms, the factor is 12.30. Thus, forbidding coupled motions by restricting the set of tunneling atoms to one atom lowers the tunneling enhancement. By contrast, this restriction increases the contributions of zero-point vibrations to the tunneling and nontunneling rates, and therefore, the rates are higher than in the larger set of tunneling atoms. The contributions of zero-point vibrations are larger for one atom because the frozen environment is like a rigid wall with a steep

dx.doi.org/10.1021/jp308526t | J. Phys. Chem. B 2012, 116, 13682−13689

potential energy valley in contrast to the softer and more flexible C−H skeleton environment of the 78-atom set. Allowing tunneling movements of C_b and $C_{5'}$ and their hydrogen atoms (active subspace with seven atoms) results in a tunneling enhancement by a factor of 12.65, already similar to the enhancement in the 78-atom set (factor 12.30). Extending the tunneling region to 11 and 23 atoms increases the enhancement factor to 14.6 and the KIE to about 16 instead of 14, see Supporting Information. Including the ribose ring of the adenosyl radical to the active subset (34- to 78-atom sets) yielded smaller enhancement factors and primary KIEs (^{2}H and ^{3}H), all similar to the results of the 78-atom set. With 34 atoms, the effective mass, μ_{eff} = 1.1636 amu, for the hydrogen transfers is basically the same as with 78 atoms, μ_{eff} = 1.1634 amu, whereas with 7, 11, and 23 active atoms, it is slightly lower (μ_{eff} = 1.1598 for seven tunneling atoms). Thus, motions of the ribose ring play some role during the tunneling of the hydrogen transfers.

These coupled motions can, on the one hand, transfer energy from the atoms moving at the ring into the movements of the transferred hydrogen atom, which would enhance the rate, and on the other hand increase the mass and reduce the tunnel rate. Two types of motions are involved in the hydrogen transfers. The classical motions (1) of the heavier carbon and oxygen atoms prepare the tunneling motions of the lighter hydrogen atoms. The larger these classical motions are, the less important is the tunneling effect. The coupled motions (2) of the ribose ring at Ado and the motions of the hydrogen atoms in the neighborhood of H_a, which reduce the tunneling rate, see results given above. These motions are coupled in the transition state and part of the tunneling motions.

Another reason for the tunneling enhancement to be smaller with one active atom is that the environment is tensed when the movement of carbon atoms (C_b and $C_{5'}$) is forbidden. A highly tensed environment leads to smaller rates for all isotopologues. The rates for 11 and 23 tunneling atoms with the ribose ring excluded from the tunneling motion (the delocalization) are smaller, see Supporting Information, than for the larger sets of atoms. Therefore, the tunneling effects dominate over the tensions when the active subspace comprises more than 34 atoms.

We can confirm the experimental conclusion from secondary tritium KIE measurements,[32] that the rehybridization of the $C_{5'}$ from planar to tetrahedral occurs before or during the transition state for the hydrogen abstraction from substrate. In the transition state both carbon atoms (C_b and $C_{5'}$) have a distorted tetrahedral coordination close to sp^3 geometry, see Figures 5 and 7.

3.4. Does a Different Step Become Rate-Determining Through a ^{1}H/^{2}H Substitution? The (measured) primary KIEs can be masked by other intermediate steps, causing the measured KIEs to be smaller than the intrinsic KIEs. A step other than hydrogen transfer could be rate limiting in case of protium. Substitution of protium by deuterium or tritium could then render the hydrogen transfer rate-limiting. As mentioned in section 3.1, the rate for $\boldsymbol{E} \rightarrow \boldsymbol{D}$ is only 16 times lower than for the direct transition $\boldsymbol{E} \rightarrow \boldsymbol{C}$ when the hydrogen transfer barrier is ignored. Thus, the carbon skeleton rearrangement would become rate-limiting if our calculations underestimated its barrier by only 7 kJ mol^{-1}. This may well be within our error bar, despite the quite high level of theory (LUCCSD(T)/MM) used to obtain the barriers. Deuterium transfer is slower by another factor of 11.5−16.8. Thus, deuterium transfer is clearly rate-limiting. The isotopically sensitive step not being fully rate-limiting is one form of masking of KIEs. It may explain why our calculated KIEs are generally somewhat larger than the experimental ones.

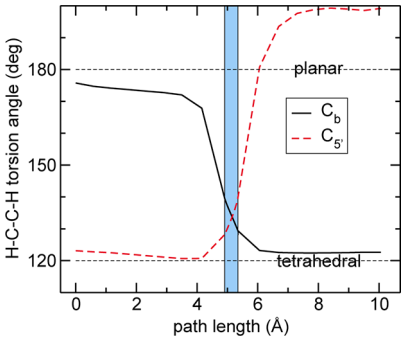

Figure 7. Dihedral angles around $C_{5'}$ and C_b showing the transition from an almost planar geometry to a distorted tetrahedral geometry during the transition $\boldsymbol{D} \rightarrow \boldsymbol{E}$. The segment of the path highlighted with blue background is the tunneling motion. The path length covers all atoms, as in Figure 6 .

Despite our frequencies being based on BP86, which underestimates the energy barriers and frequencies compared to the M06 functional or LUCCSD(T), our rates reproduce the qualitative behavior of the system. Higher frequencies would result in a larger rate. Also some rapid quench measurements hint that a slower step could mask the isotopically sensitive step in GM,[23,30,92,94,95] which would reduce the measured KIE from its intrinsic value. The change of the rate limiting step through a conformational change in the protein can be excluded as the protein moves negligibly during the catalytic cycle. The enzyme seems to modulate the transition states for the hydrogen transfers while changing the isotope effect. In the active enzyme the protein is already in a preorganized form that allows the enzyme to modulate tunneling motions, vibrations, and coupled motions. On the other hand, $\boldsymbol{A}$ is assumed to be a high energy intermediate not accumulating during the reaction.[30,31] Therefore, it is unlikely that the homolytic cleavage of AdoCbl can become rate-limiting. Further, starting at $\boldsymbol{A_0}$ or $\boldsymbol{E_0}$ could result in a higher barrier for $\boldsymbol{A_0} \rightarrow \boldsymbol{B}$ or $\boldsymbol{E_0} \rightarrow \boldsymbol{D}$. Then it would be even less likely that the carbon skeleton rearrangement could become rate-limiting.

4. CONCLUSION

We investigated the role of tunneling in the enzyme GM by QM/MM-instanton simulations. The transition $\boldsymbol{E} \rightarrow \boldsymbol{D}$ has the higher primary KIEs than $\boldsymbol{A} \rightarrow \boldsymbol{B}$. Also, the speed-up between nontunneling and tunneling rates is larger for $\boldsymbol{E} \rightarrow \boldsymbol{D}$. Thus, tunneling is more important in $\boldsymbol{E} \rightarrow \boldsymbol{D}$ than in $\boldsymbol{A} \rightarrow \boldsymbol{B}$. However, the catalysis is dominated by effects other than tunneling. The transition from an almost planar to a distorted tetrahedral geometry of the hydrogens at $C_{5'}$ and C_b occurs before and during the transition state. Primary deuterium KIEs confirm experimental findings. The barriers for the hydrogen transfers $\boldsymbol{A} \rightarrow \boldsymbol{B}$ and $\boldsymbol{E} \rightarrow \boldsymbol{D}$ match for DFT (M06) and coupled cluster (LUCCSD(T)), which shows the good predictive value of our previous results based on M06. Classical movements of the enzyme are essential to prepare the system for the tunneling transitions. The heavier atoms like oxygen or carbon show small tunneling and large classical motions during the hydrogen transfer $\boldsymbol{E} \rightarrow \boldsymbol{D}$. Allowing tunneling in different subsets of the active center showed that the motions at the

dx.doi.org/10.1021/jp308526t | J. Phys. Chem. B 2012, 116, 13682−13689

ribose ring of Ado play a role during the tunneling enhancement of the hydrogen transfers. The enzyme uses both classical and tunneling motions for a successful catalysis.

■ ASSOCIATED CONTENT

Supporting Information

Calculational details. This material is available free of charge via the Internet at http://pubs.acs.org.

■ AUTHOR INFORMATION

Corresponding Author

*E-mail: kaestner@theochem.uni-stuttgart.de.

Notes

The authors declare no competing financial interest.

■ ACKNOWLEDGMENTS

The authors thank the German Research Foundation (DFG) for financial support of the project within the Cluster of Excellence in Simulation Technology (EXC 310/1) at the University of Stuttgart. Prof. E. N. G. Marsh is acknowledged for helpful discussions.

■ REFERENCES

(1) Gamow, G. *Z. Phys.* **1928**, *51*, 204−212.
(2) Eckart, C. *Phys. Rev.* **1930**, *35*, 1303−1309.
(3) Grant, K. L.; Klinman, J. P. *Biochemistry* **1989**, *28*, 6597−6605.
(4) Knapp, M. J.; Klinman, J. P. *Eur. J. Biochem.* **2002**, *269*, 3113−3121.
(5) Antoniou, D.; Caratzoulas, S.; Kalyanaraman, C.; Mincer, J. S.; Schwartz, S. D. *Eur. J. Biochem.* **2002**, *269*, 3103−3112.
(6) Liang, Z.-X.; Klinman, J. P. *Curr. Opin. Struct. Biol.* **2004**, *14*, 648−655.
(7) Klinman, J. P. *J. Biol. Chem.* **2006**, *281*, 3013−3016.
(8) Masgrau, L.; Roujeinikova, A.; Johannissen, L. O.; Hothi, P.; Basran, J.; Ranaghan, K. E.; Mulholland, A. J.; Sutcliffe, M. J.; Scrutton, N. S.; Leys, D. *Science* **2006**, *312*, 237−241.
(9) Bandaria, J. N.; Cheatum, C. M.; Kohen, A. *J. Am. Chem. Soc.* **2009**, *131*, 10151−10155.
(10) Yoon, M.; Song, H.; Håkansson, K.; Marsh, E. N. G. *Biochemistry* **2010**, *49*, 3168−3173.
(11) Klinman, J. P. *J. Phys. Org. Chem.* **2010**, *23*, 606−612.
(12) Allemann, R. K., Scrutton, N. S., Eds. *Quantum Tunnelling in Enzyme-Catalysed Reactions*; RSC: Cambridge, U.K., 2009.
(13) Hammes-Schiffer, S. *Acc. Chem. Res.* **2006**, *39*, 93−100.
(14) Kohen, A. *Kinetic Isotope Effects as Probes for Hydrogen Tunneling in Enzyme Catalysis*; Taylor and Francis: Boca Raton, FL, 2006; pp 743−764.
(15) Nagel, Z. D.; Klinman, J. P. *Chem. Rev.* **2006**, *106*, 3095−3118.
(16) Pu, J.; Gao, J.; Truhlar, D. G. *Chem. Rev.* **2006**, *106*, 3140−3169.
(17) Warshel, A.; Sharma, P. K.; Kato, M.; Xiang, Y.; Liu, H. B.; Olsson, M. H. M. *Chem. Rev.* **2006**, *106*, 3210−3235.
(18) Kiefer, P. M.; Hynes, J. T. *Chapter Interpretation of Primary Kinetic Isotope Effects for Adiabatic and Nonadiabatic Proton-Transfer Reactions in a Polar Environment*; Taylor and Francis: Boca Raton, FL, 2006; pp 549−578.
(19) Sprecher, M.; Switzer, R. L.; Sprinson, D. B. *J. Biol. Chem.* **1966**, *241*, 864−867.
(20) Wetmore, S. D.; Smith, D. M.; Golding, B. T.; Radom, L. *J. Am. Chem. Soc.* **2001**, *123*, 7963−7972.
(21) Brunold, T. C.; Conrad, K.; Liptak, M. D.; Park, K. *Coord. Chem. Rev.* **2009**, *253*, 779−794.
(22) Sandala, G. M.; Smith, D. M.; Marsh, E. N. G.; Radom, L. *J. Am. Chem. Soc.* **2007**, *129*, 1623−1633.
(23) Chih, H.-W.; Marsh, E. N. G. *J. Am. Chem. Soc.* **2000**, *122*, 10732−10733.
(24) Marsh, E. N. G.; Patwardhan, A. *Arch. Biochem. Biophys.* **2007**, *461*, 194−199.
(25) Rommel, J. B.; Kästner, J. *J. Am. Chem. Soc.* **2011**, *133*, 10195−10203.
(26) Marsh, E. N. G. *Bioorg. Chem.* **2000**, *28*, 176−189.
(27) Buckel, W.; Golding, B. T. *Chem. Soc. Rev.* **1996**, *25*, 329−337.
(28) Chen, H.-P.; Marsh, E. N. G. *Biochemistry* **1997**, *36*, 14939−14945.
(29) Yoon, M.; Kalli, A.; Lee, H.-Y.; Håkansson, K.; Marsh, E. N. G. *Angew. Chem., Int. Ed.* **2007**, *46*, 8455−8459.
(30) Cheng, M.-C.; Marsh, E. N. G. *Biochemistry* **2005**, *44*, 2686−2691.
(31) Marsh, E. N. G.; Ballou, D. P. *Biochemistry* **1998**, *37*, 11864−11872.
(32) Cheng, M.-C.; Marsh, E. N. G. *Biochemistry* **2004**, *43*, 2155−2158.
(33) Cheng, M. C.; Marsh, E. N. G. *Biochemistry* **2007**, *46*, 883−889.
(34) Marsh, E. N. G. *Biochem. Soc. Trans.* **2009**, *37*, 336−342.
(35) Langer, J. S. *Ann. Phys. (N.Y.)* **1967**, *41*, 108−157.
(36) Miller, W. H. *J. Chem. Phys.* **1975**, *62*, 1899−1906.
(37) Callan, C. G., Jr.; Coleman, S. *Phys. Rev. D* **1977**, *16*, 1762−1768.
(38) Coleman, S. *Phys. Rev. D* **1977**, *15*, 2929−2936.
(39) Warshel, A.; Karplus, M. *J. Am. Chem. Soc.* **1972**, *94*, 5612−5625.
(40) Warshel, A.; Levitt, M. *J. Mol. Biol.* **1976**, *103*, 227−249.
(41) Sherwood, P.; de Vries, A. H.; Guest, M. F.; Schreckenbach, G.; Catlow, C. R. A.; French, S. A.; Sokol, A. A.; Bromley, S. T.; Thiel, W.; Turner, A. J.; et al. *J. Mol. Struct.: THEOCHEM* **2003**, *632*, 1−28.
(42) Senn, H. M.; Thiel, W. *Top. Curr. Chem.*; Springer: Berlin, Germany, 2007; Vol. *268*.
(43) Senn, H. M.; Thiel, W. *Curr. Opin. Chem. Biol.* **2007**, *11*, 182−187.
(44) Lin, H.; Truhlar, D. G. *Theor. Chem. Acc.* **2007**, *117*, 185−199.
(45) Riccardi, D.; Schaefer, P.; Yang, Y.; Yu, H.; Ghosh, N.; Prat-Resina, X.; Knig, P.; Li, G.; Xu, D.; Guo, H.; Elstner, M.; Cui, Q. *J. Phys. Chem. B* **2006**, *110*, 6458−6469.
(46) MacKerell, A. D., Jr.; Bashford, D.; Bellott, R. L.; Dunbrack, R. L., Jr.; Evanseck, J. D.; Field, M. J.; Fischer, S.; Gao, J.; Guo, H.; Ha, S.; et al. *J. Phys. Chem. B* **1998**, *102*, 3586−3616.
(47) MacKerell, A. D., Jr.; Feig, M.; Brooks, C. L., III *J. Comput. Chem.* **2004**, *25*, 1400−1415.
(48) Foloppe, N.; MacKerell, A. D., Jr *J. Comput. Chem.* **2000**, *21*, 86−104.
(49) MacKerell, A. D., Jr; Banavali, N. *J. Comput. Chem.* **2000**, *21*, 105−120.
(50) Smith, W.; Yong, C. W.; Rodger, P. M. *Mol. Simul.* **2002**, *28*, 385−471.
(51) Hohenberg, P.; Kohn, W. *Phys. Rev. B* **1964**, *136*, B864−B871.
(52) Kohn, W.; Sham, L. J. *Phys. Rev. A* **1965**, *140*, A1133−A1138.
(53) Dirac, P. A. M. *Proc. R. Soc. London, Ser. A* **1929**, *123*, 714−733.
(54) Slater, J. C. *Phys. Rev.* **1951**, *81*, 385−390.
(55) Vosko, S. H.; Wilk, L.; Nusair, M. *Can. J. Phys.* **1980**, *58*, 1200−1211.
(56) Becke, A. D. *Phys. Rev. A* **1988**, *38*, 3098−3100.
(57) Perdew, J. P. *Phys. Rev. B* **1986**, *33*, 8822−8824.
(58) *TURBOMOLE*, V6.0.2 2009, a development of University of Karlsruhe and Forschungszentrum Karlsruhe GmbH, 1989−2007, TURBOMOLE GmbH: Germany, 2007; available from http://www.turbomole.com.
(59) Arnim, M. v.; Ahlrichs, R. *J. Comput. Chem.* **1998**, *19*, 1746−1757.
(60) Dunning, T. H. *J. Chem. Phys.* **1989**, *90*, 1007−1023.
(61) Zhao, Y.; Truhlar, D. G. *J. Chem. Phys.* **2006**, *125*, 194101.
(62) Kendal, R. A.; Apra, E.; Bernholdt, D. E.; Bylaska, E. J.; Dupuis, M.; Fann, G. I.; Harrison, R. J.; Ju, J.; Nichols, J. A.; Nieplocha, J.; et al. *Comput. Phys. Commun.* **2000**, *128*, 260−283.
(63) Bylaska, E. J.; Jong, W. A.; Govind, N.; Kowalski, K.; Straatsma, T. P.; Valiev, M.; Wang, D.; Apra, E.; Windus, T. L.; Hammond, J.;

et al. *NWChem*, A Computational Chemistry Package for Parallel Computers, Version 5.1; Technical Report; Pacific Northwest National Laboratory, Richland, WA, 2007.
(64) Liu, Y.; Linear scaling high-spin open-shell local correlation methods. *Ph.D. thesis*, Universität Stuttgart, Germany, 2011.
(65) Liu, Y.; Werner, H.-J. 2012, to be published.
(66) Werner, H.-J.; Knowles, P. J.; Manby, F. R.; Schütz, M.; Celani, P.; Knizia, G.; Korona, T.; Lindh, R.; Mitrushenkov, A.; Rauhut, G.; et al. *MOLPRO*, version 2010.2, a package of ab initio programs, Universität Stuttgart, Germany, 2010.
(67) Amos, R. D.; Andrews, J. S.; Handy, N. C.; Knowles, P. J. *Chem. Phys. Lett.* **1991**, *185*, 256−264.
(68) Feynman, R. P. *Rev. Mod. Phys.* **1948**, *20*, 367−387.
(69) Chapman, S.; Garrett, B. C.; Miller, W. H. *J. Chem. Phys.* **1975**, *63*, 2710−2716.
(70) Mills, G.; Jónsson, H. *Phys. Rev. Lett.* **1994**, *72*, 1124−1127.
(71) Mills, G.; Jónsson, H.; Schenter, G. K. *Surf. Sci.* **1995**, *324*, 305−337.
(72) Mills, G.; Schenter, G. K.; Makarov, D. E.; Jónsson, H. *Chem. Phys. Lett.* **1997**, *278*, 91−96.
(73) Siebrand, W.; Smedarchina, Z.; Zgierski, M. Z.; Fernández-Ramos, A. *Int. Rev. Phys. Chem.* **1999**, *18*, 5−41.
(74) Smedarchina, Z.; Siebrand, W.; Fernández-Ramos, A.; Cui, Q. *J. Am. Chem. Soc.* **2003**, *125*, 243−251.
(75) Andersson, S.; Nyman, G.; Arnaldsson, A.; Manthe, U.; Jónsson, H. *J. Phys. Chem. A* **2009**, *113*, 4468−4478.
(76) Goumans, T. P. M.; Kästner, J. *Angew. Chem., Int. Ed.* **2010**, *49*, 7350−7352.
(77) Goumans, T. P. M.; Kästner, J. *Angew. Chem.* **2010**, *122*, 7508−7511.
(78) Goumans, T. P. M.; Andersson, S. *Mon. Not. R. Astron. Soc.* **2010**, *406*, 2213−2217.
(79) Richardson, J. O.; Althorpe, S. C. *J. Chem. Phys.* **2009**, *131*, 214106.
(80) Richardson, J. O.; Althorpe, S. C.; Wales, D. J. *J. Chem. Phys.* **2011**, *135*, 124109.
(81) Richardson, J. O.; Althorpe, S. C. *J. Chem. Phys.* **2011**, *134*, 054109.
(82) Meisner, J.; Rommel, J. B.; Kästner, J. *J. Comput. Chem.* **2011**, *32*, 3456−3463.
(83) Andersson, S.; Goumans, T. P. M.; Arnaldsson, A. *Chem. Phys. Lett.* **2011**, *513*, 31−36.
(84) Goumans, T. P. M. *Mon. Not. R. Astron. Soc.* **2011**, *413*, 2615−2620.
(85) Goumans, T. P. M. *Mon. Not. R. Astron. Soc.* **2011**, *415*, 3129−3134.
(86) Goumans, T. P. M.; Kästner, J. *J. Phys Chem. A* **2011**, *115*, 10767−10774.
(87) Rommel, J. B.; Kästner, J. *J. Chem. Phys.* **2011**, *134*, 184107.
(88) Gillan, M. J. *J. Phys. C: Solid State Phys.* **1987**, *20*, 3621−3641.
(89) Wigner, E. P. *Z. Phys. Chem. B* **1932**, *19*, 203−216.
(90) Kästner, J.; Carr, J. M.; Keal, T. W.; Thiel, W.; Wander, A.; Sherwood, P. *J. Phys. Chem. A* **2009**, *113*, 11856−11865.
(91) Rommel, J. B.; Goumans, M. T. P.; Kästner, J. *J. Chem. Theory Comput.* **2011**, *7*, 690−698.
(92) Chih, H.-W.; Marsh, E. N. G. *Biochemistry* **2001**, *40*, 13060−13067.
(93) Marcus, R. A.; Coltrin, M. E. *J. Chem. Phys.* **1977**, *67*, 2609−2613.
(94) Chih, H.; Roymouluik, I.; Huhta, M.; Madhavapeddi, P.; Marsh, N. *Methods Enzymol.* **2002**, 380−399.
(95) Chih, H. W.; Marsh, E. N. G. *Biochemistry* **1999**, *38*, 13684−13691.